Koistinen, Antti; Phiri, Josphat; Kesari, Kavindra; Vuorinen, Tapani; Maloney, Thaddeus

Effect of pulp prehydrolysis conditions on dissolution and regenerated cellulose pore structure

Published in:
Cellulose

DOI:
10.1007/s10570-023-05050-w

Published: 01/03/2023

Document Version
Publisher's PDF, also known as Version of record

Cellulose (2023) 30:2827–2840
https://doi.org/10.1007/s10570-023-05050-w

ORIGINAL RESEARCH

Effect of pulp prehydrolysis conditions on dissolution and regenerated cellulose pore structure

Antti Koistinen · Josphat Phiri · Kavindra Kumar Kesari · Tapani Vuorinen · Thaddeus Maloney

Received: 3 October 2022 / Accepted: 6 January 2023 / Published online: 13 January 2023

Abstract When producing regenerated cellulose materials, e.g., fibers and films, pulp fibers are first dissolved in a solvent and then regenerated in an anti-solvent. The pulp properties have a significant impact on the dissolution. This study examines the effect of pulp prehydrolysis conditions on pulp structure, subsequent dissolution in cold aqueous NaOH/ZnO solvent, and regenerated cellulose film properties. The fiber and regenerated cellulose swelling and pore structure is addressed. Once-dried kraft pulp was activated in acid hydrolysis at two temperatures, 60 and 80 °C. The hydrolysis primarily affected the cellulose degree of polymerization (DP), and its reduction dramatically improved the pulp dissolution. Surprisingly, higher hydrolysis temperature did not increase the fiber hornification. DP reduction marginally effected the pulp swelling properties but had a significant effect on the regenerated film swelling. The regenerated films contained cellulose II, and their wet porosity correlated inversely with the DP. Low hydrolysis temperature films remained more porous after critical point drying.

A. Koistinen (✉) · J. Phiri · K. K. Kesari · T. Vuorinen · T. Maloney
Department of Bioproducts and Biosystems, School of Chemical Engineering, Aalto University, 00076 Aalto, Finland
e-mail: antti.koistinen@aalto.fi

Keywords Cellulose · Dissolution · Regenerated cellulose · NaOH-water · Porosity · Thermoporosimetry

Introduction

The growing world population demands an increasing amount of raw materials to produce everyday commodities, such as food and clothing. For the clothing and textile industry, cotton is the most used raw material with an annual production of 25 million tons (Khan et al. 2020). However, the growth of cotton production is expected to stagnate in the upcoming decade (Hämmerle 2011): OECD and FAO project only 1.5% annual increase in production volumes until 2030, when global production will reach 25 million tons p.a. (OECD-FAO 2021). Cotton may be complemented with synthetic fibers; however, these polymeric fibers are manufactured from petroleum-derived constituents, and they are known to release harmful microplastics into the environment (Napper and Thompson 2016). The issue of sustainable textile fiber production is an opportunity for new man-made cellulosic fibers (MMCFs), produced from natural lignocellulosic fibers. First, the short natural cellulose fibers are dissolved and subsequently regenerated via precipitation into the long staple fibers used by the textile industry. MMCFs are more sustainable to produce than cotton as they are produced from renewable non-food cellulosic feedstocks, primarily wood

fibers (Shen and Patel 2010). In addition to MMCFs, regenerated cellulose materials are utilized in a range of applications, such as high-performance membranes for electronics or filters in desalination (Liu et al. 2021; Yuan et al. 2022).

A major constraint in all regenerated cellulose production is the dissolution of cellulose. Cellulose is a large linear homopolysaccharide, composed of (1–4) bonded β-D-glucopyranosyl units, with strong intra- and intermolecular hydrogen bonds that make it recalcitrant in most common solvents (Medronho and Lindman 2014; Budtova and Navard 2016). Cellulose dissolves only partly in aqueous NaOH and tends to rapidly gelate spotaneously; however, in the presence of additives, more complete dissolution is enabled (Budtova and Navard 2016). Zinc oxide (ZnO) has been shown to reduce the aggregation levels and slow the irreversible gelation of the dissolved cellulose solution (Egal 2006; Liu et al. 2011; Martin-Bertelsen et al. 2020; Väisänen et al. 2021). Also, urea has been shown to slow down the gelation, and the optimal NaOH/water system is composed of both urea and ZnO additives (Egal 2006). However, it is noteworthy that urea additive amounts range in 6–12 w%, whereas with ZnO only 0.7 w% is needed (Budtova and Navard 2016). This is a major advantage for preferring ZnO to urea when considering the scale-up to an industrial scale.

To enhance cellulose dissolution, its reactivity may be increased via various activation methods, aiming to increase the accessibility of the solvent to the cellulose hydroxyl groups. Common activation methods include mechanical treatments, e.g., refining and milling, to reduce the particle size, adjust the pore structure and alter the fiber morphology. Chemical activation methods are applied to remove any dissolution limiting impurities, e.g., lignin and hemicelluloses, and to optimize the cellulose molecular weight distribution—smaller and shorter molecules are easier to dissolve (Kihlman et al. 2013; Olsson and Westm 2013). These chemical methods include alkaline pretreatments and acid hydrolysis.

The role of activation is to increase cellulose reactivity; we hypothesize, however, that activation may also introduce hornification into the fibers, which causes the pores of cellulose to close and limits reactivity. Hornification occurs when fibers irreversibly lose their porosity, i.e., rewetting does not recover the lost pore structure. Hornification occurs during the manufacture of pulp, when stabilizing polymers are removed from the cell wall. Water removal in pulp drying of recycling also strongly increases hornification. While hornification is normally defined as a loss in fiber swelling, the underlying mechanism is associated with the aggregation of microfibrils (Hult et al. 2001). Hornification is known to increase with drying or processing temperature. It has also been proposed, that under some conditions, pores close from microfibril crosslinking through covalent bonds, as lactones and hemiacetals may form from reactions between carboxylic acids, aldehyde, and hydroxyl groups (Fernandes Diniz et al. 2004; Hubbe et al. 2007; Chen et al. 2011). However, the bulk of evidence indicates that irreversible hydrogen bonding is the predominant mechanism in hornification. Pönni et al. (2013) examined pulp porosity loss under acidic and alkaline aqueous environments. Using a deuteration method under FT-IR spectroscopy, they assessed cellulose accessibility in contrast to traditional water retention value measurement (WRV) which shows changes in cellulose water accessibility. They discovered that acidic pH 3 conditions (< 100 °C) cause similar accessibility loss as drying, via microfibril aggregation. Alkaline conditions at pH 12 yielded an equilibrium in aggregation, a finding that led the authors to suggest hornification to be a condition-dependent equilibrium state.

Analysis of the fiber and regenerated cellulose pore structure gives a good way to observe hornification effects, since any aggregation of fibrils should be reflected in the sample porosity. Measuring cellulose material porosity is difficult, as most porosity measurements, such as nitrogen adsorption (Brunauer et al. 1938), mercury intrusion (Gane et al. 2004; Pinnow et al. 2008; Vitas et al. 2019), and scanning electron microscopy (SEM), require the sample to be free of moisture. Water removal under ordinary conditions causes the pores to collapse. This problem may be mitigated by exchanging the water, through an intermediate solvent, to carbon dioxide, which is then evaporated above its critical point (Lovikka et al. 2016). Thus, surface tension effects are eliminated and dry fibers with largely intact pores can be generated. Another approach is to perform porosity measurements directly on wet samples using a suitable technique such as solute exclusion (Stone and Scallan 1968; Lin et al. 1987; Flournoy et al. 1991), NMR (Li et al. 1995) or thermoporosimetry.

Thermoporosimetry is a method for determining the pore size distribution (PSD) of mesoporous materials. The method is based on observing the solid–liquid phase transition of water in confined geometry (Maloney and Paulapuro 1999; Riikonen et al. 2011); water molecules in pores experience a melting point depression. The PSD of pulp fibers falls mostly in the mesoscopic range and can be measured on a suitably accurate differential scanning calorimeter (DSC) with an appropriate thermoporosimetry algorithm. Thermoporosimetry has been earlier applied to various cellulosic materials: recently, the porosity of a plant-based hydrogel composed of cellulose nanofibrils, lignin nanoparticles and tragacanth gum was examined with DSC thermoporosimetry (Polez et al. 2022). Thermoporosimetry has been used in characterizing cellulosic membranes manufactured from nano-fibrillated cellulose (Orsolini et al. 2015), however, regenerated cellulose material in membranes has not earlier been thermoporometrically examined.

In this paper, we examined how acid hydrolysis activates and possibly hornifies kraft pulp fibers. The effect of the hydrolysis conditions on the dissolution of the pulps was qualitatively analyzed. To understand how hydrolysis induced hornification affects precipitation, the dissolved and semi-dissolved pulps were regenerated into films, whose structure was analyzed. Our target was to find out if the structural changes introduced into the fibers in the prehydrolysis phase carry through to the regenerated cellulose structure.

Materials

Bleached softwood kraft pulp (BSWKP) was received as dry industrial pulp sheets. BSWKP was a spruce and pine mixture. The pulp carbohydrate composition was determined following the protocol by Sluiter et al. (2011) with high-performance anion exchange chromatography with pulsed amperometric detection (HPAEC-PAD) in a Dionex ICS-3000 system (Thermo Fisher Scientific, US). The samples were analyzed in duplicate. Following the Janson formula (Janson 1970), cellulose and hemicellulose content were calculated according to the amount of measured monosaccharides. The pulp had a hemicellulose content of 18.9% (Table 1).

The BSWKP molecular mass distribution was measured using a size-exclusion chromatography method reported earlier (Pitkänen and Sixta 2020). The analysis was performed with a Dionex Ultimate 3000 HPLC module (Thermo Fisher Scientific Inc., US), equipped with a Shodex DRI (RI-101) detector (Showa Denko, Japan), and a Viscotek/Malvern SEC/MALS 20 multi-angle light-scattering (MALS) detector (Malvern Panalytical Ltd., UK). Four PLgel MIXED-A columns (Agilent Technologies Inc., US) with 0.76 mL/min flow rate were used. The sample was dissolved in the eluent (0.9% LiCl in DMAc) using a solvent exchange procedure (water/acetone/DMAc) described earlier (Potthast et al. 2002). Two injections of 100 µL were analyzed. MALS and DRI detector constants were determined, and detector calibrations were performed as reported by (Pitkänen and Sixta 2020). The molecular weight distribution had a bimodal profile with a broad shoulder at larger molecular weights. The lower molar mass peak represents the hemicellulose fraction, whereas the higher mass peak corresponds to cellulose distribution. The molecular size characteristics are reported in Table 1.

The cellulose degree of polymerization (DP) was calculated from weight-average molecular mass M_w using

$$\mathrm{DP}_w = M_w/162 \quad (1)$$

The pulp was cold disintegrated according to ISO 5263–1:2004. To activate for dissolution, the pulp was hydrolyzed in 0.5 M sulfuric acid following a procedure by Battista (1950). 20 g (bone dry) of disintegrated BSWKP at 40% solids content was weighed in a 500 mL glass bottle. 400 g of pre-heated 0.5 M sulfuric acid was added to the pulp. Subsequently, the bottle was closed and placed into a heated oven. After

Table 1 BSWKP structural characteristics

Mn (kDa)	Mw (kDa)	Mz (kDa)	PDI	DPw	DP > 2000 (%)	DP < 100 (%)	Chemical composition (%)			
							Cel	Xyl	Gluc	Lignin
87	305	712	3.5	1882	30.4	1.1	80.6	10.9	8.0	0.5

the desired hydrolysis time (see Table 2), the sample was washed with deionized water until the pulp conductivity was less than 10 µS/cm.

To study the hornification caused by the hydrolysis, two sample sets were made at two temperatures, 60 and 80 °C. Parameters used for hydrolysis are shown in Table 2. The sample name is composed of used hydrolysis temperature (60 or 80 °C) and the determined degree of polymerization (DP).

The limiting viscosities of the hydrolyzed samples were measured according to SCAN-CM 15:99. The DP was estimated from the limiting viscosity value according to

$$DP = 0.75[\mu]^{1/0.905} \quad (2)$$

where [µ] is the limiting viscosity value. (Immergut et al. 1953) This formula for DP is widely used for estimating the molecular size from intrinsic viscosities (Kes and Christensen 2013; Kihlman et al. 2013; Palme et al. 2016). The fiber dimensions and fines content were measured using Kajaani FiberLab fiber dimensions analyzer (Metso Automation, Finland).

The water retention value (WRV) was measured according to ISO 23714:2014.

Methods

Cellulose dissolution and film preparation

Hydrolyzed pulp samples were dissolved in a NaOH/ZnO solvent system.

NaOH/ZnO storage solution with 18 wt% NaOH and 3 wt% ZnO content was prepared beforehand by first dissolving NaOH pellets in water. Then, in the released heat of NaOH dissolution, the ZnO powder dissolved effectively leaving no visible granules. The stock solution was stored at –20 °C.

The hydrolyzed pulp (dry matter content ca. 20 wt%) was diluted with deionized (DI) water and NaOH/ZnO stock solution was added to achieve 7.8 wt% NaOH, 1.3 wt% ZnO and 7.0 wt% cellulose consistency dope in a glass beaker. The mixture was stirred with a glass rod, and the beaker was held in ice-water. The dopes were placed in the freezer (–20 °C) for at least overnight. The sample was thawed with the degas program of a Thinky Mixer ARE-250 planetary centrifuge (Thinky Corporation, Japan) for 20 min at 2000 rpm, removing air bubbles from the mixture (Reyes et al. 2022). To avoid gelation, the resulting dope was analyzed immediately.

The dissolved cellulose samples were precipitated into regenerated cellulose (RC) films via film casting: First, approximately 2 g of dope was applied on a 10 × 10 cm glass slide. A second 10 × 10 cm glass was pressed on top of the first slide. When DP was < 500 DP, dissolution was sufficiently completely, and a thin, homogeneous dope layer was formed. DP > 500 pulps formed a heterogeneous mixture of undissolved fibers in the NaOH/ZnO solvent. Subsequently, the two glasses were slid apart, leaving a thin dope layer on each glass slide. The slides were immersed dope-side upwards in 12 w% sulfuric acid for at least 5 min. Regenerated cellulose films precipitated and with the help of tweezers were detached from the glass panes. The films were washed with DI water and stored in air-tight bags between moist blotting papers. The films were stored in refrigeration (+4 °C).

Table 2 Hydrolysis temperatures and times used

Sample ID	Hydrolysis temperature (°C)	Hydrolysis time (h)
BSWKP	N/A	0
60DP800	60	2
60DP480	60	16
60DP330	60	48
80DP710	80	1
80DP340	80	4
80DP200	80	24

Critical point drying (CPD)

Critical point drying (CPD) was used to prepare dry samples with intact pore structures. First, a film was submerged in 50 vol% acetone for 5 min with stirring. This was repeated twice in neat, dry acetone. The sample was stored overnight in a sealed bottle with acetone and zeolite absorbent.

For the films, the acetone was exchanged with liquid CO_2 in a Leica EM CPD300 critical point drier (Leica Microsystems GmbH, Germany) for 60 cycles. Subsequently, the CO_2 was brought to a supercritical state, vented, and only CO_2 at atmospheric pressure remained. For N_2 sorption analysis, the film samples

were immediately transferred to the sorption vials. For scanning electron microscope (SEM) imaging, the same protocol was used, except the exchange was performed for 18 cycles.

For the pulp samples used in SEM analysis, the acetone exchange was done in dialysis membranes (Spectra/Por® 6 RC tubing, MWCO 50 kDa), in 25, 50, 75 and 100 vol% acetone stirred for 45 min. The samples were left overnight in dry acetone before CPD drying, sputtering, and imaging.

Microscopy

The BSWKP and hydrolyzed samples were imaged in cross-polarized light with an optical microscope prior dissolution and immediately after thawing the dissolved in the NaOH/ZnO solvent.

For SEM analysis, the samples were prepared in a low humidity room (< 10% relative humidity). CPD dried samples were mounted onto double-sided carbon tape and were sputtered with gold–palladium to form a 4 nm layer conductive layer on the sample surface. The images were captured using a Zeiss Sigma VP SEM (Carl Zeiss, Germany) with a 2.0 kV accelerating voltage.

Pore analysis

The PSD and specific surface area (SSA) of the CPD regenerated cellulose films were calculated from the N_2 adsorption isotherms with the application of the Barrett-Joyner-Halenda (BJH) and Brunauer-Emmitt-Teller (BET) models, respectively. The isotherms were obtained using Micromeritics TriStar II 3020 (Micromeritics Instrument Corporation, USA). A preheating program of 50 °C for 30 min was used to expel any water absorbed during sample transfer from CPD to the sorption instrument.

The pulp and film pore structure was studied in the wet state using thermoporosimetry. The thermoporosimetric method is based on that water in sufficiently small cell wall cavities will melt at depressed temperatures. The relationship between the diameter of the pore (D) and the melting temperature depression (ΔT_m) is given by the simplified Gibbs–Thomson equation

$$D = \frac{k}{\Delta T_m}, \tag{3}$$

where k has been earlier determined to equal 43 K·nm (Maloney 2015). A Mettler DSC3 + (Mettler Toledo, Switzerland) differential scanning calorimeter was used in the measurements. The PSD was calculated from the freezing exotherms in the range of −20° to −0.2 °C under non-supercooling conditions. This is the temperature range where pore water in cellulosic materials melts. −0.2 °C is the maximum temperature before the melting of bulk water begins to interfere with the measurement. This corresponds to about $D = 200$ nm, which is the upper limit where pores can be accurately determined. Temperature calibration was done with mercury and distilled water, and enthalpy calibration with distilled water. About a monolayer of water at the pore-cellulose interface does not freeze at any temperature. This nonfreezing water (NFW) can be used as a measure of the state of hydration of the material. The NFW was determined as described earlier (Maloney 2015). SA in the mesopore range was calculated from the thermoporosimetry PSD assuming a cylindrical geometry of pores.

Both CPD/N_2 sorption and thermoporosimetry primarily supply information about the mesopore structure of the cellulosic samples. This is the dominant pore range for many cellulosic materials. However, the presence of micro- and macropores, outside the range of these methods, may be important in some instances.

Raman spectroscopy

Raman spectra were collected from the hydrolyzed pulps and RC samples. Prior to analysis, samples were dried in atmospheric air. Raman spectra were acquired with Renishaw inVia™ confocal Raman microscope (Renishaw, United Kingdom) using a 578 nm laser with a 20× air objective. 0.5 s integration time was used, and 1024 accumulations were gathered. The spectra were baseline corrected and normalized with the Renishaw Wire 5.3 software (highest intensity band at 1096 cm^{-1}).

Results and discussion

Samples with varying degrees of polymerization were produced to analyze the effect of temperature on sample hornification during acid hydrolysis. The hypothesis was that a higher temperature hydrolysis would lower the DP faster and cause hornification to the fiber. To assess this effect, samples with equal DP were produced in two temperatures, 60 and 80 °C. The BSWKP and hydrolyzed pulp properties are summarized in Table 3. Based on limiting viscosity results, the BSWKP had a DP of 1178, which decreased during acid hydrolysis in both temperatures. When cellulose is subjected to an acid, the glycosidic linkages break between the anhydroglucose units.

The starting fiber length was 2.13 mm (length weighted average), and this decreased in hydrolysis to 0.67 mm for the 80DP200 sample. The fines content was about constant in hydrolysis until the 80DP200 sample. For this sample, the conditions were aggressive enough to break down the fibrillar structure leading to a significant change in WRV from around 0.97 to 1.11 g/g. The other samples experienced only slight WRV loss from the initial 0.97 g/g value.

The pore volumes are reported in Table 3. Only slight changes to wet porosity of the hydrolyzed fibers were detected with DSC. 80DP200 sample showed 16% smaller pore volume. The pore volume decreased from the acid hydrolysis, indicating hornification: for example, for samples 60DP330 and 80DP340, their pore volumes decreased by 7.9%, using the hydrolysis times reported in Table 2. This suggests that there is some fibril aggregation in the hydrolysis. The NFW, on the other hand, dropped only from 0.28 to 0.26 g/g, which is on the limits of detectability. This indicates that the hydrated surface area of the samples changes only to a small extent in the hydrolysis.

Thus, at the highest hydrolysis level, the fiber begins to break down into fibril aggregates, which are internally more aggregated, but still preserving a monolayer of bound water (NFW) over most of the elementary fibril surfaces. This is a good example, of why it is important to consider the length scale of the measurement when considering fiber swelling. The water sorption of the parent fiber may behave differently than the finer scale fibril structure.

The fiber morphologies were examined with SEM and optical microscopy, see Fig. 1. The morphology remained unchanged after hydrolysis for all samples except for 80DP200, which had deteriorated, and shortened.

Dissolved cellulose morphology

The hydrolyzed pulps and BSWKP reference were mixed in NaOH/ZnO solvent, placed in the freezer at −20 °C overnight, and thawed. The dissolution state was studied with optical microscopy imaging, see Fig. 2. Although optical microscopy does not distinguish the state of molecular dissolution, it is a simple and quick method to visualize macroscale dissolution. BSWKP, 60DP800 and 80DP710 samples did not dissolve, but showed only heterogeneous swelling (ballooning) of the pulp fibers. Medium DP samples exhibited dissolution and loss of the fiber structure. Low DP samples were visually dissolved to nearly invisible, however, clear undissolved fragments are visible under cross-polarized light. The degree of dissolution may be classified from no change,

Table 3 Properties of pulps

Sample	DP	Fiber length (mm)	Fines content (%)	WRV (g/g)	Moisture content (g/g)	NFW (g/g)	Pore volume (mL/g)	Mesopore SA (m^2/g)
BSWKP	1178 ± 1.6	2.13	2.37	0.97 ± 0.01	1.26 ± 0.08	0.28 ± 0.01	0.76 ± 0.02	330
60DP800	800 ± 4.4	2.04	3.25	0.97 ± 0.02	1.32 ± 0.08	0.28 ± 0.05	0.70 ± 0.05	310
60DP480	479 ± 1.8	2.01	3.13	0.95 ± 0.03	1.39 ± 0.13	0.26 ± 0.07	0.69 ± 0.04	320
60DP330	330 ± 1.2	2.04	2.85	0.96 ± 0.02	1.31 ± 0.03	0.27 ± 0.02	0.70 ± 0.002	340
80DP710	711 ± 0.3	2.12	2.89	0.95 ± 0.01	1.51 ± 0.05	0.26 ± 0.03	0.72 ± 0.03	330
80DP340	339 ± 2.1	2.03	3.12	0.95 ± 0.002	1.30 ± 0.08	0.29 ± 0.04	0.69 ± 0.05	300
80DP200	196 ± 1.0	0.67	15.27	1.11 ± 0.006	1.35 ± 0.06	0.26 ± 0.02	0.64 ± 0.05	280

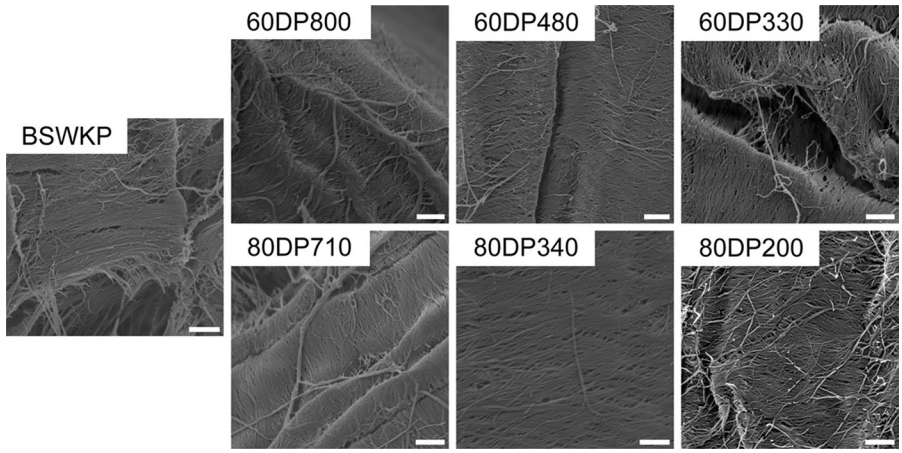

Fig. 1 SEM images of pulp fibers. Reference BSWKP and hydrolyzed pulp SEM images reveal only small changes in fiber properties from hydrolysis. The scale bar represents 500 nm length

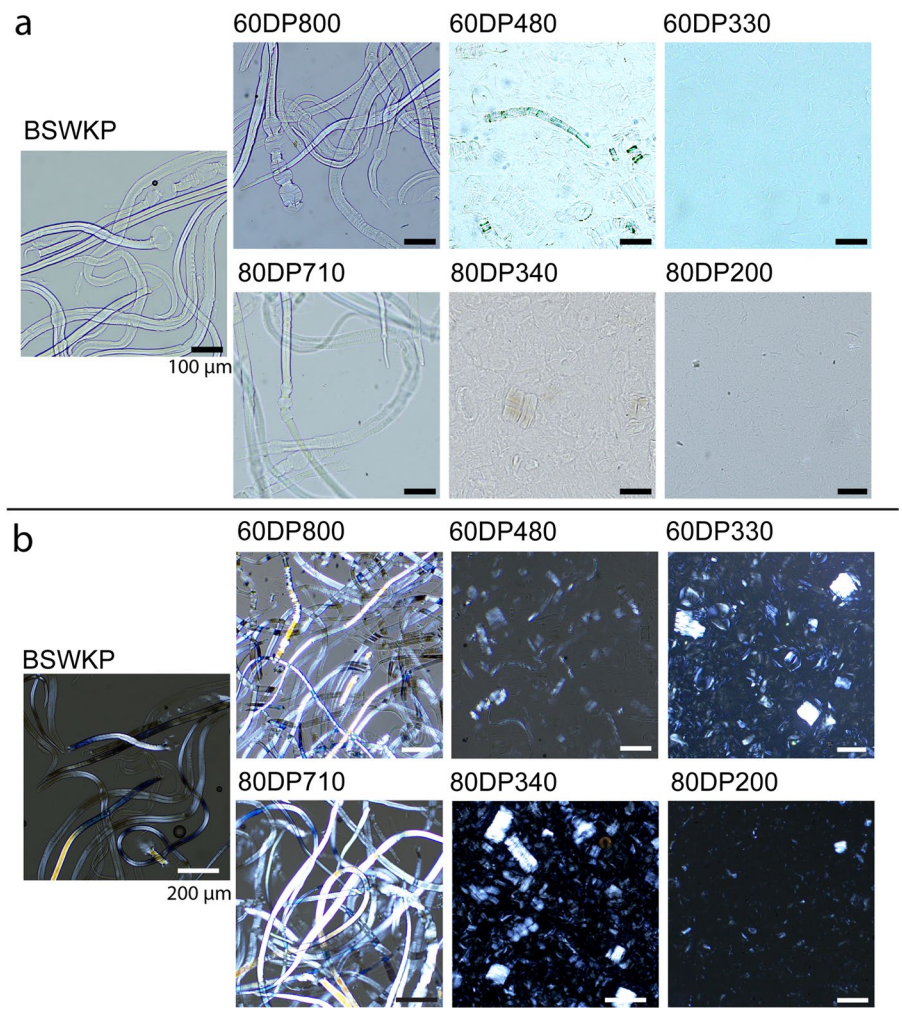

Fig. 2 Optical microscopy **a** and cross-polarized light **b** images of pulps dissolved in NaOH/ZnO

ballooning, and fragmentation to complete apparent dissolution (Cuissinat and Navard 2006). The DP appears to have a pronounced effect on the dissolution. Similar findings are reported in previous works (Kihlman et al. 2012). The reference and samples with DP > 500 sample preserved their fibrillar shape during dissolution: only heterogeneous swelling with ballooning was seen. All samples that had a DP < 500 were somewhat dissolved; however, the undissolved residue was observed in all samples. In a perfect dissolution, all the cellulose chains would separate from each other, leading to a molecular-disperse solution with no visible structures (Medronho and Lindman 2015).

As cellulose is exposed to an aqueous NaOH/ZnO solvent, the cellulose molecules become solvated and lose their capability to form intramolecular hydrogen bonds. The solvation degree varies from heterogeneous swelling to complete dissolution, where the cellulose molecules are completely liberated from intramolecular bonds. (Cuissinat and Navard 2006).

Interestingly, the fiber porosity loss had little influence on dissolution capability. This indicates that the NaOH/ZnO solvent can easily penetrate the pulp after the acid hydrolysis. The acid hydrolysis induced hornification was only minor in terms of affecting the pulp reactivity. It appears that the favorable increase in entropy, brought about by the reduced DP (Lindman et al. 2010), outweighs any accessibility issues brought about by fibril aggregation.

Raman spectroscopy

The cellulose crystallinity and allotropic state were studied with Raman spectroscopy. In lignocellulosic samples, ordered crystalline cellulose produces strong and narrow peaks, whereas disordered compounds contribute with broad and weak signals in Raman spectra (Agarwal and Ralph 1997). Previously, Raman spectroscopy has been successfully applied to determine cellulose crystallinity for both cellulose I and cellulose II allomorphs (Agarwal et al. 2010, 2021). The ordered unit cells have different spectral characteristics: cellulose I can be distinguished from peak intensity at 380 cm^{-1} (Agarwal et al. 2010), whereas this peak is absent in cellulose II, where a distinct peak is seen at 577 cm^{-1} (Agarwal et al. 2021).

Figure 3 shows the Raman spectra in region 250–1500 cm^{-1} for pulp and the RC samples. The pulp fiber samples show a peak at 380 cm^{-1} wavenumbers. The regenerated samples miss the peak at 380 cm^{-1}, but a peak is present at 577 cm^{-1}. Thus, as pulp is dissolved in aqueous NaOH/ZnO, and subsequently precipitated in H_2SO_4, cellulose regenerates into cellulose II. Samples that did not dissolve but underwent heterogeneous swelling were also converted to cellulose II, i.e., mercerization took place.

Films

Film pore structure

The dissolved cellulose in NaOH/ZnO solvent system was precipitated as regenerated cellulose (RC) films in 12 w-% sulfuric acid. The PSD and related information were evaluated from the films in the wet state, with thermoporosimetry and in the dry state, with CPD and N_2 sorption. The results are summarized in Table 4 and Fig. 4. The unhydrolyzed reference showed an 105% increase in pore volume, 69%

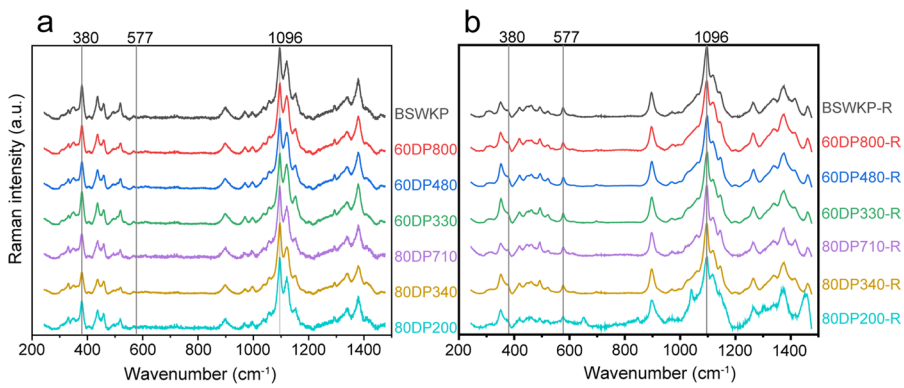

Fig. 3 Hydrolyzed pulps **a** and regenerated cellulose **b** Raman spectra. The transition from cellulose I to cellulose II is seen at 380 cm^{-1} peak disappearing and 577 cm^{-1} peak appearing in cellulose II (**b**)

Table 4 Dry and wet porosity results of RC films

Sample	Critical point dried samples		Water saturated samples		
	BJH pore volume (mL/g)	BET cumulative surface area (m^2/g)	NFW (g/g)	Pore volume (mL/g)	Mesoporous surface area (m^2/g)
BSWKP-R	–	–	0.48 ± 0.01	1.56 ± 0.05	700
60DP800-R	0.73	290 ± 0.38	0.38 ± 0.01	1.84 ± 0.16	880
60DP480-R	1.35	340 ± 1.0	0.52 ± 0.04	2.08 ± 0.22	830
60DP330-R	1.67	410 ± 1.5	0.48 ± 0.02	1.98 ± 0.22	820
80DP710-R	0.67	240 ± 0.72	0.39 ± 0.02	1.74 ± 0.09	850
80DP340-R	1.10	340 ± 1.66	0.49 ± 0.02	2.11 ± 0.12	880
80DP200-R	1.31	300 ± 0.39	0.48 ± 0.00	2.27 ± 0.22	880

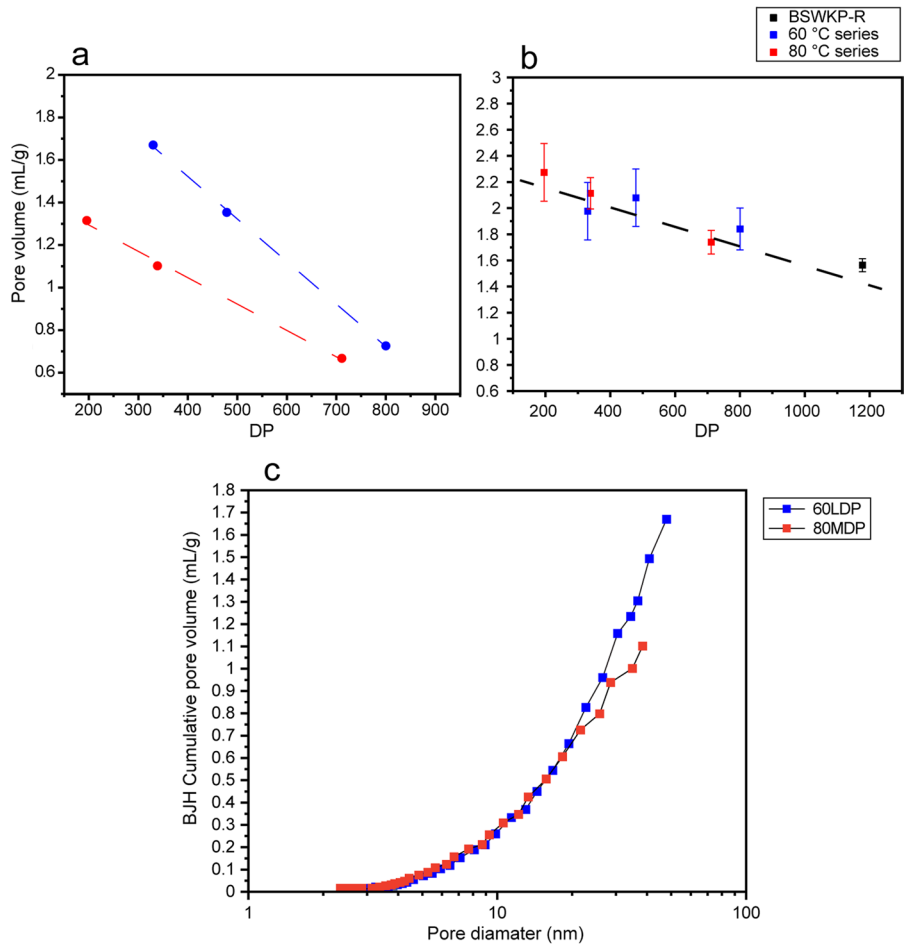

Fig. 4 Both dry pore volume (**a**: BJH pore volume from N_2 sorption measurement) and wet pore volume (**b**: thermoporosimetry) increases as pulp molecular size decreases. In the dry state, the pore volume of 60 °C films were higher than the 80 °C. Comparison of 60DP330 and 80DP340 film pore volume distribution **c** shows that with nearly equal molecular size cellulose, film from 60 °C hydrolyzed pulp has 0.6 ml/g larger cumulative porosity, of which all differences occur at pores larger than 20 nm

in surface area, and 71% increase in NFW undergoing the freeze–thaw treatment in NaOH/ZnO as hydrolyzed pulps.

From thermoporosimetry, the pore volume correlates inversely with DP over the range of 2.3 mL/g at the lowest DP, to 1.6 mL/g for the reference sample.

The more complete dissolution of cellulose at lower DP leads to higher swelling in the regenerated films. For the results from water saturated samples, the data collapses to a single line (Fig. 4b). However, the correlation of DP with pore volume of CPD samples depended on the hydrolysis temperature. The samples hydrolyzed at lower temperature (60 °C) had a distinctly higher pore volume at any given DP (Fig. 4a). We suspect that structural differences in the regenerated films become evident when the samples are dried through a solvent exchange process. The lower pore volume of the 80 °C set would be consistent with the notion that the higher hydration temperature has increased the hornification in the samples. However, it is still unclear why this effect is visible in the dry state, but not in the wet state. The PSD in Fig. 4c shows the increased pore volume at lower hydrolysis temperature, which is associated with the larger mesopores, in the range of 20 to 50 nm.

From the hydrated films, the non-freezing water was determined. The wet films had an increased NFW content when compared to the hydrolyzed pulp the film was made from. This is explained by cellulose I conversion to the cellulose II allomorph, which has a larger crystalline unit cell, capable to hold intracrystalline water (Wada et al. 2010). In cellulose I, the NFW is mostly located on the surface of the microfibrils. Thus, the fibrils are not swollen. In this study, the NFW increased from around 0.28 g/g to 0.4–0.5 g/g. Additionally, the regenerated cellulose surface increased compared to pulp surface area prior dissolution: mesoporous surface area for wet pulp fibers was in the range of 280–300 m^2/g, and 700–880 m^2/g for wet films. As surface area grows, it is capable to hold more NFW on the film surface (Riikonen et al. 2011; Maloney 2015). Interestingly, the NFW remains high after regeneration of the films; indicating the fibrils remain swollen after the removal of alkali and regeneration (Wada et al. 2010).

Regenerated film morphology

The film morphology was observed with SEM imaging and are reported in Fig. 5 and Fig. 6. Samples that did not dissolve under the freeze–thaw treatment precipitated into complex structures of heterogeneously swollen kraft fibers accompanied with regenerated porous structures (Fig. 5, large pictures). Samples with DP < 500 coagulated as homogeneous films that also had undissolved fibrous fractions affixed to the film; in 60DP800 and 80DP710 films, a composite structure of partially dissolved fibers bound by a matrix of porous regenerated cellulose is visible. In 60DP480 and 80DP340 films some

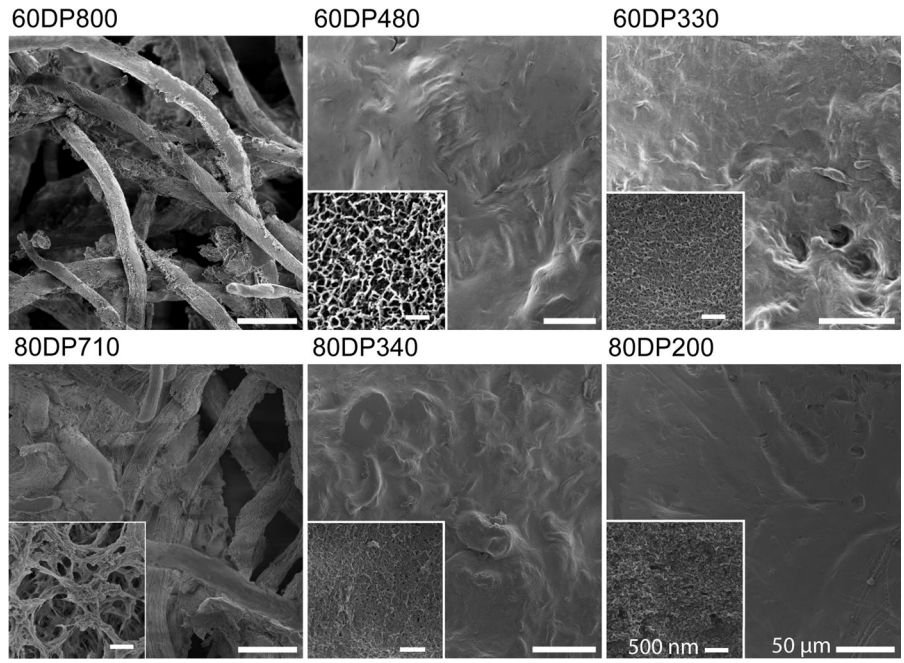

Fig. 5 SEM images of regenerated cellulose film surface show clear differences in film structure. Inset images depict the porous structure on the film surface

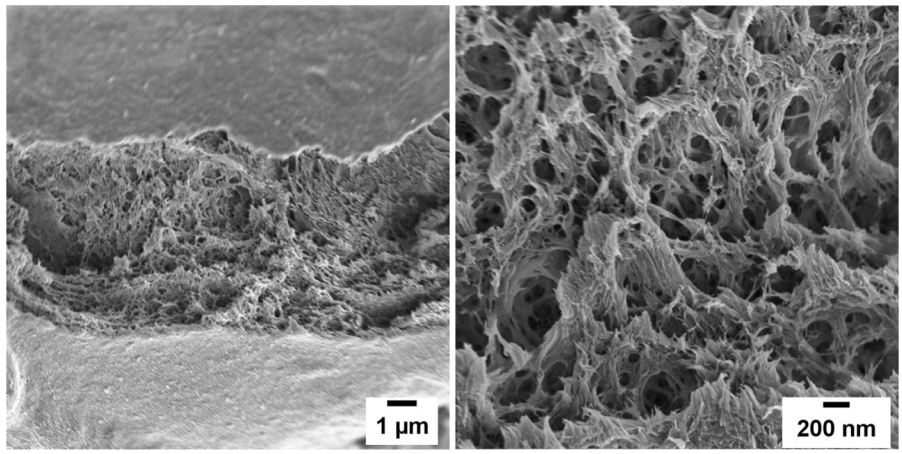

Fig. 6 Regenerated cellulose film internal and external pore architecture. Left: several micrometers wide tear on the film surface reveals the film internal pore structure. Right: Magnification on the internal structure

undissolved fractions are visible. In 60DP330 film a rough surface morphology is seen, whereas 80DP200 is smooth, with some undissolved residues affixed in the regenerated cellulose plane. The morphology differences were minimal between the two hydrolysis temperatures.

The pore surface pore architecture is seen in Fig. 5 (inset images); surface pore diameter decreases as sample DP decreases. However, N_2 adsorption and thermoporosimetric porosity increased as DP increased. The regenerated cellulose SEM images of a crack in the film surface in Fig. 6 reveals differences between the superficial and internal pore structure: the film surface has relatively smaller pore structure than the inside, resembling a skin–core morphology. Furthermore, the internal pores exhibit a longitudinal formation, which potentially originated from the film fabrication as the top glass pane was slid off the bottom pane, causing orientation prior precipitation in non-solvent. The visible pores appear to be a bimodal distribution: one set of pores is in the range 100–200 nm and second set 200–500 nm. The material is clearly macroporous. Since both CPD/N_2 and thermoporosimetry are sensitive to mesopores, we must recognize that in our analysis we have detected only part of the distribution. The situation is made more complicated because it is clear the pores on the surface of the sample are smaller than in the interior. The PSD is wide, heterogeneous, and structurally complicated. Further studies should employ a broader range of analysis methods to deal with these issues. The skin–core structure has been reported to result from high cellulose concentration at the non-solvent/solvent interface at the initiation of coagulation (Medronho and Lindman 2015).

Conclusions

The hydrolysis time and temperature primarily affect the cellulose DP. The reduction in DP has only a small effect on the swelling properties of the pulp, until the point the fiber structure disintegrates from the acid hydrolysis. However, reduced DP dramatically improves pulp dissolution. The wet pore volume of regenerated films produced from the hydrolyzed samples correlated inversely with DP: lower DP led to higher swelling films. The films contained a high fraction of cellulose II, which was more highly hydrated than the cellulose I in the hydrolyzed fibers. We expected that higher hydrolysis temperature would have a substantial effect on fiber and film properties, since increased temperature often leads to higher hornification. However, this effect was only slightly visible in the fiber properties or in the wet film properties. Surprisingly, when the wet films were critical-point-dried and analyzed with N_2 sorption porosimetry, the effect of the hydrolysis temperature was clearly visible. Lower hydrolysis temperature led to higher pore volume, independent of DP. Mostly this was due to changes in the pores above about 20 nm. This affect may be due to hornification (aggregation of fibrils), changes to the molecular weight distribution (Ceccherini et al. 2021), or other morphological factors not analyzed in this study.

Acknowledgements This work made use of the Aalto University Bioeconomy Facilities as well as the Aalto University Nanomicroscopy Center (Aalto NMC) facilities. Ms. Rita Hatakka is thanked for the guidance performing the carbohydrate analysis and Dr Leena Pitkänen for molecular weight distribution analysis.

Author's contributions AK: Conceptualization, Writing–original draft, Investigation, Formal analysis, Visualization. JP: Software, Validation, Writing–review and editing. KK: Investigation, Writing–review and editing. TV: Conceptualization, Methodology, Writing–review and editing. TM: Conceptualization, Methodology, Writing–review and editing, Supervision.

Funding Open Access funding provided by Aalto University. This work was supported by Aalto University.

Declarations

Conflict of interest The authors declare that they have no competing interests.

References

Agarwal UP, Ralph SA (1997) FT-raman spectroscopy of wood: Identifying contributions of lignin and carbohydrate polymers in the spectrum of black spruce (Picea mariana). Appl Spectrosc 51:1648–1655. https://doi.org/10.1366/0003702971939316

Agarwal UP, Ralph SA, Baez C, Reiner RS (2021) Detection and quantitation of cellulose II by Raman spectroscopy. Cellulose 28:9069–9079. https://doi.org/10.1007/s10570-021-04124-x

Agarwal UP, Reiner RS, Ralph SA (2010) Cellulose I crystallinity determination using FT-Raman spectroscopy: univariate and multivariate methods. Cellulose 17:721–733. https://doi.org/10.1007/s10570-010-9420-z

Battista OA (1950) Hydrolysis and crystallization of cellulose. Ind Eng Chem 42:502–507. https://doi.org/10.1021/ie50483a029

Brunauer S, Emmett PH, Teller E (1938) Adsorption of gases in multimolecular layers. J Am Chem Soc 60:309–319. https://doi.org/10.1021/ja01269a023

Budtova T, Navard P (2016) Cellulose in NaOH–water based solvents: a review. Cellulose 23:5–55. https://doi.org/10.1007/s10570-015-0779-8

Ceccherini S, Ståhl M, Sawada D et al (2021) Effect of enzymatic depolymerization of cellulose and hemicelluloses on the direct dissolution of prehydrolysis kraft dissolving pulp. Biomacromol 22:4805–4813. https://doi.org/10.1021/acs.biomac.1c01102

Chen YM, Wan JQ, Huang MZ et al (2011) Influence of drying temperature and duration on fiber properties of unbleached wheat straw pulp. Carbohydr Polym 85:759–764. https://doi.org/10.1016/j.carbpol.2011.03.041

Cuissinat C, Navard P (2006) Swelling and dissolution of cellulose part 1: free floating cotton and wood fibres in N-methylmorpholine-N-oxide-water mixtures. Macromol Symp 244:1–18. https://doi.org/10.1002/masy.200651201

Egal M (2006) Structure and properties of cellulose/NaOH aqueous solutions, gels and regenerated objects. PhD thesis, École Nationale Supérieure des Mines de Paris/Cemef, Sophia-Antipolis

Fernandes Diniz JMB, Gil MH, Castro JAAM (2004) Hornification-Its origin and interpretation in wood pulps. Wood Sci Technol 37:489–494. https://doi.org/10.1007/s00226-003-0216-2

Flournoy DS, Kirk K, Highley TL (1991) Wood decay by brown-rot fungi: changes in pore structure and cell wall volume. Holzforschung 45:383–388. https://doi.org/10.1515/hfsg.1991.45.5.383

Gane PAC, Ridgway CJ, Lehtinen E et al (2004) Comparison of NMR cryoporometry, mercury intrusion porosimetry, and DSC thermoporosimetry in characterizing pore size distributions of compressed finely ground calcium carbonate structures. Ind Eng Chem Res 43:7920–7927. https://doi.org/10.1021/ie049448p

Hämmerle FM (2011) The cellulose gap (the future of cellulose fibres). Lenzinger Berichte 89:12–21

Hubbe MA, Venditti RA, Rojas OJ (2007) What happens to cellulosic fibers during papermaking and recycling? A review. Bioresources 2:739–788. https://doi.org/10.15376/biores.2.4.739-788

Hult EL, Larsson PT, Iversen T (2001) Cellulose fibril aggregation—an inherent property of kraft pulps. Polymer 42:3309–3314. https://doi.org/10.1016/S0032-3861(00)00774-6

Immergut EH, Ranby BG, Mark HF (1953) Recent work on molecular weight of cellulose. Ind Eng Chem 45:2483–2490. https://doi.org/10.1021/ie50527a036

Janson J (1970) Calculation of the polysaccharide composition of wood and pulp. Pap Puu 52:323–328

Kes M, Christensen BE (2013) A re-investigation of the Mark-Houwink-Sakurada parameters for cellulose in Cuen: A study based on size-exclusion chromatography combined with multi-angle light scattering and viscometry. J Chromatogr A 1281:32–37. https://doi.org/10.1016/j.chroma.2013.01.038

Khan MA, Wahid A, Ahmad M et al (2020) World cotton production and consumption: an overview. In: Ahmad S,

Hasanuzzaman M (eds) Cotton production and uses, 1st edn. Springer Singapore, Singapore

Kihlman M, Aldaeus F, Chedid F, Germgård U (2012) Effect of various pulp properties on the solubility of cellulose in sodium hydroxide solutions. Holzforschung 66:601–606. https://doi.org/10.1515/hf-2011-0220

Kihlman M, Medronho BF, Romano AL et al (2013) Cellulose dissolution in an alkali based solvent: influence of additives and pretreatments. J Braz Chem Soc 24:295–303. https://doi.org/10.5935/0103-5053.20130038

Li TQ, Henriksson U, Ödberg L (1995) Determination of pore volume in cellulose fibers by the pulsed gradient spin-echo NMR technique. J Colloid Interface Sci 169:376–379. https://doi.org/10.1006/JCIS.1995.1046

Lin JK, Ladisch MR, Patterson JA, Noller CH (1987) Determining pore size distribution in wet cellulose by measuring solute exclusion using a differential refractometer. Biotechnol Bioeng 29:976–981. https://doi.org/10.1002/bit.260290809

Lindman B, Karlström G, Stigsson L (2010) On the mechanism of dissolution of cellulose. J Mol Liq 156:76–81. https://doi.org/10.1016/j.molliq.2010.04.016

Liu W, Budtova T, Navard P (2011) Influence of ZnO on the properties of dilute and semi-dilute cellulose-NaOH-water solutions. Cellulose 18:911–920. https://doi.org/10.1007/s10570-011-9552-9

Liu X, Xiao W, Tao T et al (2021) Transparent, smooth, and sustainable cellulose-derived conductive film applied for the flexible electronic device. Carbohydr Polym 260:117820

Lovikka VA, Khanjani P, Väisänen S et al (2016) Porosity of wood pulp fibers in the wet and highly open dry state. Microporous Mesoporous Mater 234:326–335. https://doi.org/10.1016/j.micromeso.2016.07.032

Maloney T (2015) Thermoporosimetry of hard (silica) and soft (cellulosic) materials by isothermal step melting. J Therm Anal Calorim 121:7–17. https://doi.org/10.1007/s10973-015-4592-2

Maloney T, Paulapuro H (1999) The formation of pores in the cell wall. J Pulp Pap Sci 25:430–436

Martin-Bertelsen B, Andersson E, Köhnke T et al (2020) Revisiting the dissolution of cellulose in NaOH as "seen" by X-rays. Polymers (basel) 12(2):1–15. https://doi.org/10.3390/polym12020342

Medronho B, Lindman B (2014) Competing forces during cellulose dissolution: from solvents to mechanisms. Curr Opin Colloid Interface Sci 19:32–40. https://doi.org/10.1016/j.cocis.2013.12.001

Medronho B, Lindman B (2015) Brief overview on cellulose dissolution/regeneration interactions and mechanisms. Adv Colloid Interface Sci 222:502–508. https://doi.org/10.1016/j.cis.2014.05.004

Napper IE, Thompson RC (2016) Release of synthetic microplastic plastic fibres from domestic washing machines: Effects of fabric type and washing conditions. Mar Pollut Bull 112:39–45. https://doi.org/10.1016/j.marpolbul.2016.09.025

OECD-FAO (2021) OECD-FAO agricultural outlook 2021–2030. OECD Publish. https://doi.org/10.1787/4ad4cf3a-en

Olsson C, Westm G (2013) Direct dissolution of cellulose: background, means and applications. In: de Ven T, Godbout L (eds) Cellulose fundamental aspects. IntechOpen, London, pp 143–178

Orsolini P, Michen B, Huch A et al (2015) Characterization of pores in dense nanopapers and nanofibrillated cellulose membranes: a critical assessment of established methods. ACS Appl Mater Interfaces 7:25884–25897. https://doi.org/10.1021/ACSAMI.5B08308/SUPPL_FILE/AM5B08308_SI_001.PDF

Palme A, Theliander H, Brelid H (2016) Acid hydrolysis of cellulosic fibres: comparison of bleached kraft pulp, dissolving pulps and cotton textile cellulose. Carbohydr Polym 136:1281–1287. https://doi.org/10.1016/j.carbpol.2015.10.015

Pinnow M, Fink HP, Fanter C, Kunze J (2008) Characterization of highly porous materials from cellulose carbamate. Macromol Symp 262:129–139. https://doi.org/10.1002/masy.200850213

Pitkänen L, Sixta H (2020) Size-exclusion chromatography of cellulose: observations on the low-molar-mass fraction. Cellulose 27:9217–9225. https://doi.org/10.1007/s10570-020-03419-9

Polez RT, Morits M, Jonkergouw C et al (2022) Biological activity of multicomponent bio-hydrogels loaded with tragacanth gum. Int J Biol Macromol 215:691–704. https://doi.org/10.1016/J.IJBIOMAC.2022.06.153

Pönni R, Kontturi E, Vuorinen T (2013) Accessibility of cellulose: Structural changes and their reversibility in aqueous media. Carbohydr Polym 93:424–429. https://doi.org/10.1016/j.carbpol.2012.12.025

Potthast A, Rosenau T, Buchner R et al (2002) The cellulose solvent system N,N-dimethylacetamide/lithium chloride revisited: the effect of water on physicochemical properties and chemical stability. Cellulose 9:41–53. https://doi.org/10.1023/A:1015811712657

Reyes G, King AWT, Koso TV et al (2022) Cellulose dissolution and gelation in NaOH(aq) under controlled CO_2 atmosphere: supramolecular structure and flow properties. Green Chem 24:8029–8035. https://doi.org/10.1039/d2gc02916b

Riikonen J, Salonen J, Lehto V (2011) Utilising thermoporometry to obtain new insights into nanostructured materials review part 1. J Therm Anal Calorim. https://doi.org/10.1007/s10973-010-1167-0

Shen L, Patel MK (2010) Life cycle assessment of man-made cellulose fibres. Lenzinger Berichte 88:1–59

Sluiter A, Hames B, Ruiz RO et al (2011) Determination of structural carbohydrates and lignin in biomass. Lab Anal Proced 1617(1):1–16

Stone JE, Scallan AM (1968) A structural model for the cell wall of water-swollen wood pulp fibres based on their accessibility to macromolecules. Cellul Chem Technol 2:343–358

Väisänen S, Ajdary R, Altgen M et al (2021) Cellulose dissolution in aqueous NaOH–ZnO: cellulose reactivity and the role of ZnO. Cellulose. https://doi.org/10.1007/s10570-020-03621-9

Vitas S, Segmehl JS, Burgert I, Cabane E (2019) Porosity and pore size distribution of native and delignified beech wood determined by mercury intrusion porosimetry. Materials 12:1–13. https://doi.org/10.3390/ma12030416

Wada M, Ike M, Tokuyasu K (2010) Enzymatic hydrolysis of cellulose I is greatly accelerated via its conversion to the cellulose II hydrate form. Polym Degrad Stab 95:543–548. https://doi.org/10.1016/j.polymdegradstab.2009.12.014

Yuan H, Hao R, Sun H et al (2022) Engineered Janus cellulose membrane with the asymmetric-pore structure for the superhigh-water flux desalination. Carbohydr Polym 291:119601